Multi-Line Breaker for HVdc Applications

Multi-Line Breaker for HVDC Applications

E. Kontos, *Student Member*, T. Schultz, L. Mackay, *Student Member*,
L. Ramirez-Elizondo, *Member*, C. M. Franck, *Senior Member* and P. Bauer, *Senior Member*

***Abstract*—This paper presents a breaker arrangement concept, the Multi-Line Breaker (MLB), for the protection of multi-terminal high voltage dc (MTdc) networks. Based on the design of a hybrid breaker, the MLB is an economically attractive solution for the protection of multiple dc lines in nodal connection using a single main breaker path. By using commutation units, the MLB directs the fault current through the main breaker in a unidirectional way, irrespective of the fault location. Hence, this study presents the design requirements for the MLB, regarding both hardware and control, and evaluates its operation within a grid. For this reason, a four-terminal half-bridge MMC-based MTdc grid in radial configuration was used and pole-to-ground dc fault conditions were investigated. The dc fault response of the grid with one MLB at the central node is compared to the respective response of the grid when one hybrid breaker is employed at each dc line. The simulations show that the MLB is feasible and that the overall MTdc grid fault response for the two protection systems is very similar. As a result, the design advantages of the MLB make it a promising solution for the dc fault isolation in MTdc grids.**

***Index Terms* – Fault currents, HVdc circuit breakers, HVdc converters, HVdc transmission, Multiterminal networks.**

I. Introduction

High voltage direct current (HVdc) technology is important for long distance power transmission due to its inherent advantages over its ac counterpart, e.g. lower losses, no reactive compensation and high controllability [1]. As of now, the use of voltage-source converters (VSC) and especially of multi-level modular converters (MMC) has been limited, due to their complexity in terms of control and protection [2], [3]. On this basis, research is being conducted for the realization of small multi-terminal HVdc (MTdc) grids [4], [5], as well as more meshed grid topologies in the future [6]–[8].

Due to the absence of a natural zero-crossing of the dc current, the isolation of a fault on a dc line is more difficult than in case of faults in ac grids [9]. Very fast transients and high overcurrents, occurring in case of dc faults, are likely to damage the involved equipment and are more difficult to break [10]. To isolate dc faults, breakers need to be rated for high current (e.g. 12 pu) [11]. Moreover, there are high requirements for the dissipation of the energy stored in HVdc lines [12] and the time constraints are very stringent, especially when it comes to grid operation, where the dc fault needs to be isolated before it affects the operation of the 'healthy' part of the grid [13].

Many dc breaker topologies have been proposed to solve the protection problem in HVdc grids [14]–[17]. Among them solid-state breakers and hybrid mechanical breakers, as proposed in the literature [18], appear to be the most promising technologies, mainly due to their low fault interruption times. Apart from the time response, on-state losses are also a very important issue [19]. Due to the large scale transmission of bulk energy, the system has to have high efficiency during normal operation. Hybrid breakers have a better performance, as they consist of the Nominal Current Path (NCP) with low resistance that is used during normal operation, the Current Commutation Path (CCP) and the Energy Absorption Path (EAP). In general there are several different hybrid breaker topologies proposed [20]–[23], which can be grouped into two main types, i.e. one type uses Ultra-Fast Disconnectors (UFD), while the second type uses mechanical circuit breakers as the switching element. For the first type, there are different implementations, one of which can be described as Load Commutation Switch - Mechanical Breaker (LCS-MB), using an LCS/UFD in parallel with a stack of semiconductors, which can be controllably switched on and off. This principle was presented by ABB under the name 'proactive hybrid circuit breaker' [20]. The general structure of a hybrid breaker is presented in Fig. 1.

Although it is claimed by HVdc manufacturers that circuit breakers are readily available, multi-terminal HVdc networks are not yet realized in large-scale, apart from two projects which were commissioned in China, which do not have dc circuit breakers yet [24], [25]. Among other problems, cost of protection poses a significant challenge towards dc grids [26]. In case of hybrid breakers, the use and cost of the different paths involved in the breaking process need to be optimized. Past studies have proposed different concepts in the direction of breaker design and possible implementation into networks, including the idea of component sharing [27], [28] to decrease the cost. However, more elaborate studies are necessary, which need to examine the hardware and control implementation of the dc breakers in MTdc networks, taking into account the boundary conditions that influence the fault interruption time requirements.

The idea to use a circuit arrangement to replace several circuit breaker at a dc node by only one, i.e. the Multi-Line Breaker (MLB), was presented in a patent of the authors [29]. This is realized by minimizing the number of CCP and EAP paths needed and also the number of the involved switching elements within the breaker, while offering a bidirectional fault isolation capability. Based on the basic operation principle and path structure of proposed dc breakers, the MLB optimizes the number of protection assets by using only one unidirectional CCP and one EAP for more than one dc lines, as shown in Fig. 2. To achieve that, two NCPs connected at each dc line are controlled to drive the dc fault current through the main breaking paths, whereas at normal operation they facilitate the bidirectional power flow in the dc grid. Unlike [28], the MLB design is simple and highly modular, facilitating the easy expansion to more interconnecting lines.

A dynamic analysis of the application of the same circuit arrangement as a bidirectional circuit breaker on a single line was presented in [30]. This is a special case that is also mentioned in [29]. However, in this case, the use of individual circuit breakers on each line is proposed instead of only one unidirectional main breaker to protect the complete node.

This paper's main contribution is the design and in depth analysis of the MLB based on the idea presented in [29]. This constitutes a generalized concept and is elaborated hereby with the structure of the LCS-MB. This paper goes beyond previous studies [29], [30], providing a thorough investigation of the hardware and control implementation of the MLB. More specifically, the switching actions of different switches in the breaker paths and the effect of the timing on the MLB operation are studied. Moreover, an economic analysis is provided, taking into account the relative costs of components and the scalability of the breaker to more lines in order to quantify the advantages the MLB breaker arrangement brings compared to the use of individual breakers for each line. Additionally, this study presents a sizing methodology of the main breaker components for the chosen case study. Finally, the MLB performance is evaluated using an example of an MTdc grid and is compared to the performance of individual dc breakers for each dc line. Table I is used for quick reference of the most commonly used abbreviations in this paper.

The paper is structured as follows: Section II presents the MLB breaker concept, explaining the hardware and software implementation needs, analyzing the cost of the protection system in comparison to a dc grid protected by hybrid circuit breakers. Section III presents the case study used to evaluate the effectiveness of the breaker, along with the specifications of the main grid assets. In Section IV, the results for the MLB fault response are compared to the results obtained using hybrid breakers and the main differences in the transient behavior are elaborated. Finally, in Section V, conclusions are drawn on the feasibility of the MLB concept.

TABLE I
ABBREVIATIONS OF COMMON TERMS.

LCS-MB	Load Commutation Switch - Mechanical Breaker
MLB	Multi-Line Breaker
NCP	Nominal Current Path
CCP	Current Commutation Path
EAP	Energy Absorption Path
LCS	Load Commutation Switch
UFD	Ultra-Fast Disconnector

II. MULTI-LINE BREAKER CONCEPT IMPLEMENTATION

A. Hardware Requirements

Based on the review analysis performed in [23], the LCS-MB, as proposed in [31] and shown in Fig. 3, appears to be faster than other hybrid breaker concepts proposed in the literature, although probably more expensive. Therefore, in the present study, the LCS-MB is chosen as the reference case for evaluation of the MLB concept.

Based on the LCS-MB design, the MLB uses an Ultra Fast mechanical Disconnector (UFD) and a Load Commutation Switch (LCS), which constitute the NCP, to connect each line to each of the two busbars, which, hereafter, will be identified as 'a' and 'b', as shown in Fig. 2. Busbars and connections can introduce stray inductances that affect the current commutation speed between branches. Hence, care has to be taken, when designing the circuit breaker. However, if the design is optimized for low stray inductance, the commutation time can be considered significantly shorter than the total operation time of the breaker. As a result, in this study, the busbar inductances are not considered in the analysis of the MLB. In this configuration, a single CCP and EAP is sufficient to break the dc fault current. It has to be noted that the system designer can decide to oversize the CCP and EAP ratings, based on the number of dc faults that the MLB needs to deal

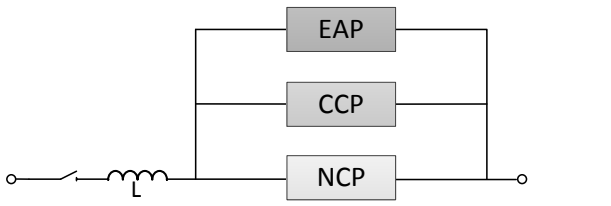

Fig. 1. Hardware structure of a hybrid breaker.

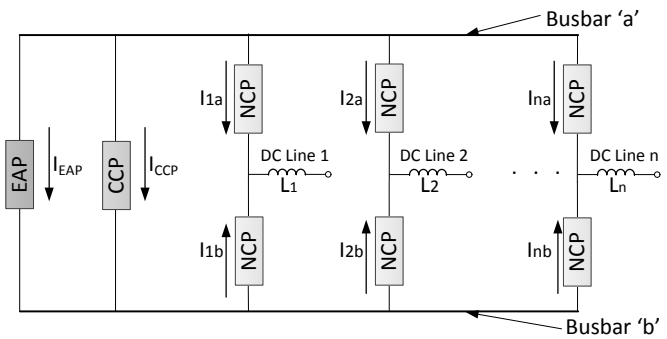

Fig. 2. Hardware structure of a Multi-line breaker (MLB).

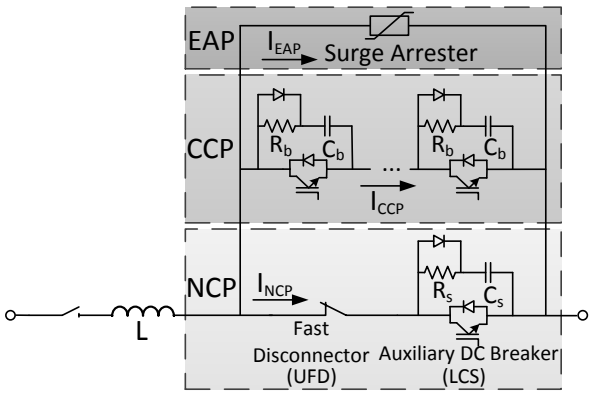

Fig. 3. LCS-MB breaker with its three paths.

with simultaneously. A schematic of the implemented version of the MLB is presented in Fig. 5.

The main difference between the MLB concept and existing breaker concepts is that it allows the protection of multiple lines at the same time. By using only one main breaker circuit in a unidirectional scheme, the MLB significantly reduces the number of switching elements needed and subsequently the protection system cost. It has to be noted that to isolate the dc fault in the MLB arrangement, more individual switching actions are required than in case of the LCS-MB. However, as these occur in parallel, the total fault interruption time is not affected. Moreover, as this might affect reliability, it has to be taken into account, when specifying the requirements for UFDs for the MLB. Moreover, the necessary volume of the station, housing the protection system, is also reduced, further bringing down the cost and the construction complexity of the project, which are more important in case of offshore constructions.

B. Control Requirements

In case of an LCS-MB the control sequence is straightforward, as shown in Fig. 4. As soon as a fault is detected, the LCS of the NCP opens and the current is commutated to the CCP. When i_{NCP} drops to residual current level, the UFD opens. Finally, when UFD is fully open and has established dielectric strength (approximately within 2 ms), the switches in the CCP are switched off and the current is commutated to the EAP, where the energy is dissipated.

Based on the control sequence of the LCS-MB, the MLB control is designed. More specifically, Fig. 5 shows the MLB control sequence in case of a three-line dc connection, when the fault occurs on line 2. It has to be noted that in case of the MLB, a jitter of the UFD opening times will probably occur. As a result, a dead-time is required in the design to allow the synchronization of the UFDs opening. Fig. 6 presents the times at which control events occur. In the time symbols used in the following analysis, the subscripts 'f' and 'nf' denote the faulty and not-faulty line respectively, while the subscripts '(a)' and '(b)' indicate the bus to which the NCP unit is connected.

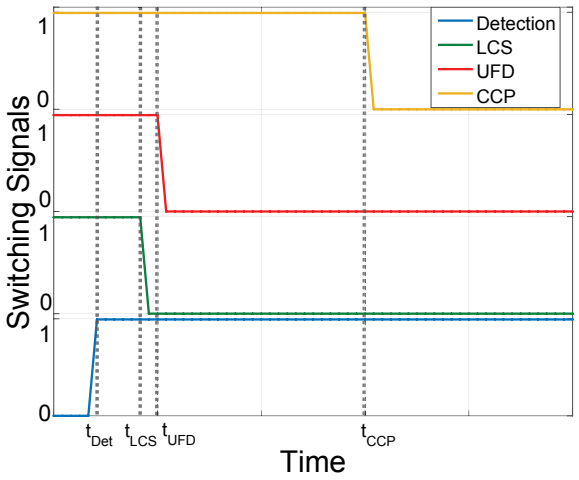

Fig. 4. Switching sequence hybrid. '1' and '0' values indicate the 'on' and 'off' states respectively.

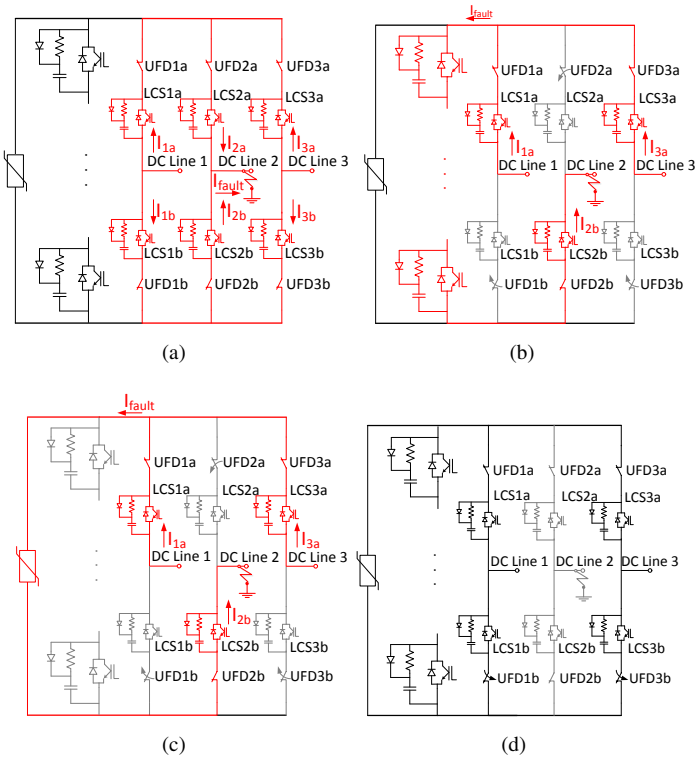

Fig. 5. Control sequence of the MLB illustrated for a configuration with three attached lines.

Four control steps can be distinguished for the dc fault ride-through:

1) Initially, all switches of the MLB are closed. As soon as a dc fault occurs on line 2, the capacitances of the healthy lines discharge through the fault. Therefore, there is a high overcurrent flowing from the connected healthy lines through the node into the fault, e.g. dc line 2 (I_{2a} and I_{2b}), as shown in Fig. 5(a).
2) After the faulty line is detected at t_{Det}, the faulty line is disconnected from bus 'a' by opening the NCP unit (UFD2a/LCS2a) ($t_{\mathrm{LCS\text{-}f(a)}}$ and $t_{\mathrm{UFD\text{-}f(a)}}$), while the healthy lines are disconnected from bus 'b' by opening the respective NCP units (UFD1b/LCS1b and UFD3b/LCS3b) ($t_{\mathrm{LCS\text{-}nf(b)}}$ and $t_{\mathrm{UFD\text{-}nf(b)}}$). This commutates the complete fault current into the unidirectional CCP. This step is shown in Fig. 5(b).
3) When the mechanical disconnectors on the NCP units, which were opened in the previous step, are fully open and have established their dielectric strength ($\sim$ 2 ms), the switches in the CCP open (t_{CCP}) and the current is commutated to the surge arrester in the EAP path, where the energy is dissipated, as presented in Fig. 5(c).
4) Once the fault current flowing to the faulty line drops to residual current level, the NCP unit (UFD2b/LCSb) opens ($t_{\mathrm{LCS\text{-}f(b)}}$ and $t_{\mathrm{UFD\text{-}f(b)}}$). In this way, dc line 2 is fully isolated from the rest of the network. At this moment, the NCP paths (UFD1b/LCS1b and

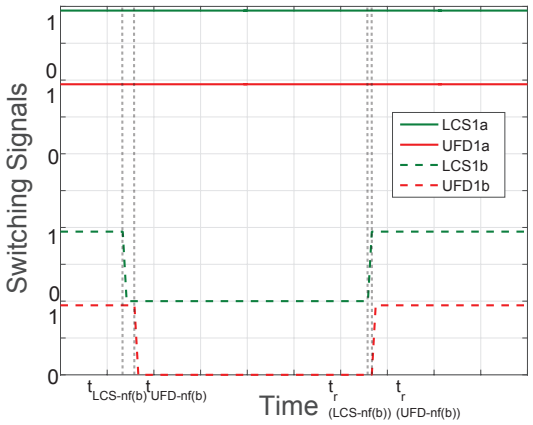

(a)

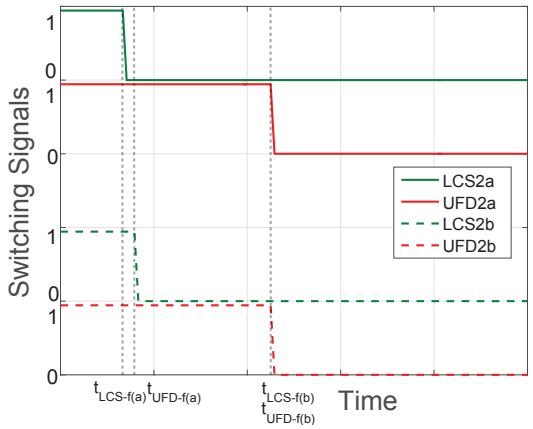

(b)

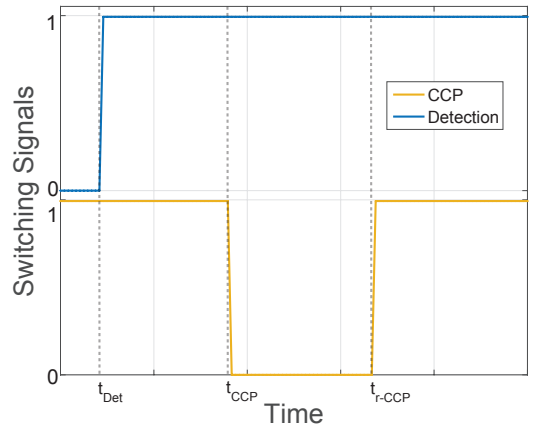

(c)

Fig. 6. Pole-to-ground - Switching Sequence MLB1: (a) Healthy line path (1); (b) Faulty line path (2); (c) Main Breaker path and Fault signals. '1' and '0' values indicate the 'on' and 'off' states respectively.

UFD3b/LCS3b) connecting the 'healthy' lines to bus 'b' reclose ($t_{r(\text{LCS-nf(b)})}$ and $t_{r(\text{UFD-nf(b)})}$) and CCP recloses as well ($t_{\text{r-CCP}}$), as in Fig. 5(d). In this way, normal operation is restored in the grid and the MLB is ready to isolate a possible fault in another line.

The aforementioned control strategy is independent of the number of lines interconnected through the MLB and therefore, the breaker is highly modular with minimum changes.

C. Economic considerations

Hereby, a comparative analysis of the costs of the different protection systems is made taking into account the cost of the involved paths. To allow the comparison, it is assumed that the paths that are used for the MLB are exactly the same as the ones used for the individual hybrid breakers, which is the worst-case scenario for the cost comparison. It is assumed that c_{NCP} is the cost of the nominal current path, c_{CCP} is the cost of the current commutation path and c_{EAP} is the cost of the energy absorption path. Assuming n is the number of interconnected lines, cases $n = 1$ or 2 refer to a point-to-point connection. Therefore, the following analysis is made for $n \geq 3$. The total cost of the LCS-MB breaker is calculated as:

$$\Sigma C_{\text{LCS-MB}} = n \cdot (c_{\text{NCP}} + c_{\text{CCP}} + c_{\text{EAP}}) \tag{1}$$

Respectively, the cost of the MLB is given by:

$$C_{\text{MLB}} = 2 \cdot n \cdot c_{\text{NCP}} + c_{\text{CCP}} + c_{\text{EAP}} \tag{2}$$

To make a comparison between the two costs for n lines, the fraction of the path costs is used. Assuming that:

$$\frac{c_{\text{NCP}}}{c_{\text{CCP}}} = a \tag{3}$$

and

$$\frac{c_{\text{EAP}}}{c_{\text{CCP}}} = b \tag{4}$$

As a result, the cost fraction $\frac{\Sigma C_{\text{LCS-MB}}}{C_{\text{MLB}}}$ of the two technologies depends on both n, a and b. In case the breakers have unidirectional breaking capability, the cost fraction is given by:

$$\frac{\Sigma C_{\text{LCS-MB}}}{C_{\text{MLB}}} = \frac{n(a+1+b)}{2na+1+b} \tag{5}$$

while assuming that LCS-MB has bidirectional breaking capability, this cost fraction becomes larger, as the c_{CCP} of the LCS-MB is double compared to the MLB, namely:

$$\frac{\Sigma C_{\text{LCS-MB}}}{C_{\text{MLB}}} = \frac{n(a+2+b)}{2na+1+b} \tag{6}$$

Fig. 7 shows the trend of the costs for the technologies using unidirectional breaking capability. Assuming that the same CCP and EAP paths can be used in both breaker technologies, while only the number of involved NCP paths changes, the ratio between the cost of NCP and the combined costs of CCP and EAP becomes valuable in the analysis and is calculated as:

$$\frac{c_{\text{NCP}}}{c_{\text{CCP}} + c_{\text{EAP}}} = \frac{a}{b+1} \tag{7}$$

The use of MLB is justified if the following conditions apply: (i) three or more lines are interconnected through the MLB and (ii) the cost of the NCP is lower than 0.6 of the combined cost of CCP and EAP. The more lines and the higher the cost ratio between the NCP and CCP+EAP, the higher the individual LCS-MB breakers capital investment is compared to the MLB solution. It has to be noted that the

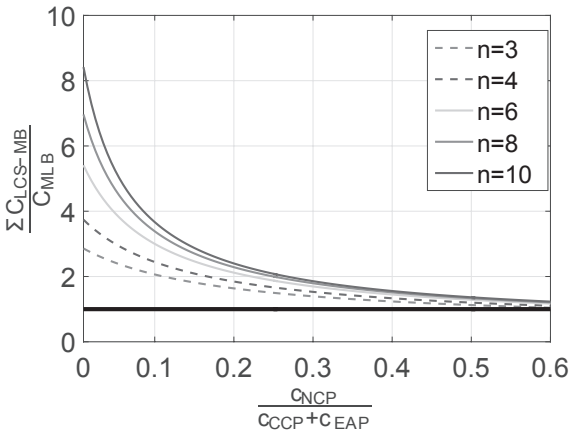

Fig. 7. Sensitivity analysis of the cost of MLB over LCS-MB breakers and cost ratio between NCP and the combined cost of CCP+EAP, for different number of lines n. The thick black line, at y=1, indicates the break-even point between the two breaker costs.

comparison is theoretical, neglecting the details of the cost division between the different components involved. In case of bidirectional LCS-MB capability, the cost ratio of the two technologies would be higher.

III. MTdc Network Case Study

The performance of the different circuit breaker concepts is evaluated in the present study using a four-terminal radially-connected MTdc network with half-bridge MMC stations as presented in Fig. 8. As shown, the MTdc network operates in asymmetric monopolar configuration with metallic return.

In normal operation, MMC1 is used to control the dc voltage operational level of the MTdc grid, while MMC2, MMC3 and MMC4 control their ac active power. The return path is grounded at the dc side of the MMC1 station. In case of the MMC station, no bulky capacitors are used on the dc side of the stations and thus, the dc fault currents exhibit lower initial peak [10], [11]. As a result, no large limiting reactors are necessary on the dc side of the MMC, as the MMC arm reactors are designed accordingly to limit the rate of rise of the current in case of terminal faults. However, limiting reactors are necessary on the node of the radial connection and thus, they are taken into account in the dc breaker design. The main MTdc network parameters are shown in Table II.

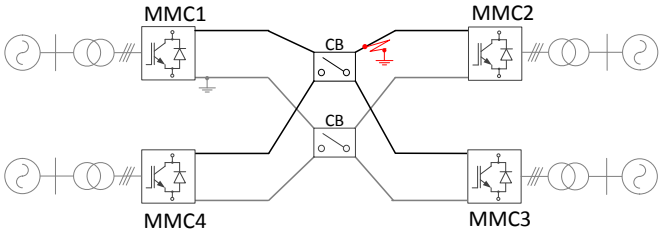

(a)

Fig. 8. Layout of the analyzed radial MTdc network with 4 terminals with a pole-to-ground dc fault.

TABLE II
MTDC NETWORK PARAMETERS.

Network parameters	Unit	Value
MMC rated power (S_{MMC})	MVA	1200/1200/600/600
MTdc voltage (V_{dc})	kV	320
DC cable resistance (R_{cable})	Ω/km	0.0195
DC cable inductance (L_{cable})	mH/km	0.2
DC cable capacitance (C_{cable})	nF/km	220
DC cable length (d1/d2/d3/d4)	km	50
Transformer voltage ratio (VSC1/VSC2)	kV	380/160 (Y_0-Δ)
Transformer voltage ratio (VSC3/VSC4)	kV	33/160 (Y_0-Δ)
Transformer rated power (S_{T})	MVA	1200/1200/600/600
Transformer leakage inductance (L_{T})	pu	0.05

A. MMC Model

This paper focusses on the protection of an MTdc network that is based on half-bridge MMC converter stations, which do not have inherent fault current blocking capability. The aim of this study is to evaluate the MLB operation and present a proof-of-concept. Therefore, 9-level Half-bridge MMCs are used in this study for simplicity purposes and their specifications are presented in Table III. The MMC parameters are chosen following the design procedure described in [32]. It has to be noted that the submodule capacitance is calculated using the energy storage requirement of the MMC [33]. For the MTdc network analysis, a detailed simulation model which accounts for the MMC-HVdc stations switching behavior is implemented using the SimPowerSystems toolbox of Matlab/Simulink. All the converters share the same control structure, regardless of their control mode within the MTdc network, as presented in Fig. 9 [34]. Moreover, the dc lines are modelled using cascaded pi-equivalent cable sections.

The converter valves are only tripped by the overcurrent protection which is implemented at each converter arm. As soon as one of the arm currents exceeds the defined current threshold, the fault signal is sent to the converter controller and the converter trips. The threshold of the overcurrent protection is defined at 2 pu [18] and its absolute value depends on the rating of each converter station.

TABLE III
MMC PARAMETERS.

MMC specifications	Unit	Value
Energy stored per power unit (W_{rated}/S_{MMC})	J/VA	30e-3
Arm inductance (L_{arm})	pu	0.1
Arm resistance (R_{arm})	pu	0.01
Number of SMs per arm (N)	-	8
Carrier frequency (f_{c})	Hz	600
Sampling frequency (f_{s})	kHz	20

B. Circuit Breaker Model

The circuit breakers used in this study are modelled using the SimPowerSystems toolbox of Matlab/Simulink. A simple selective fault detection method is used based on the current direction during a dc fault. A dc line overcurrent threshold is chosen equal to the threshold of the IGBT valves of the converter station, i.e. 2 pu. As soon as a fault occurs on a dc line, the line capacitance discharges through the fault. As a result, current from all lines flows towards the dc fault point, as it is shown in Fig. 10. As soon as this current exceeds the defined protection threshold, the faulty line is identified and the actions for its isolation are initiated. In case of a breaker or bus failure, back-up protection can be provided either by disconnecting all the lines connected to the node using the breakers on the other ends of the lines or by operating the ac breakers at the converter terminals. However, this would result in a disconnection of the node, which would lead to a substantial power flow disturbance. Therefore, backup protection is an issue that has to be considered before building the grid and has severe consequences for both MLB and LCS-MB schemes.

In the design of the circuit breaker, several parameters need to be taken into account. First of all, the LCS on each path is structured as a 3x3 IGBT array with 15 kV voltage rating and 15 kA current rating. The LCS RC snubber circuit parameters are selected based on these ratings to protect the LCS IGBTs at all instants of operation [35]. Moreover, the voltage drop across the UFD must remain very small until full contact separation, which is estimated at 2 ms. The design of the UFD and its contact motion characteristics affect the increase in dielectric strength during opening. In this study, for simplicity reasons, linear opening motion and homogeneous field conditions are assumed. This results in a linear increase of the dielectric strength of the UFD of 320 kV/ms. Finally, the CCP has 192 IGBTs grouped in 4 stacks.

The circuit breaker parameters for the two technologies under study are presented in Table IV. In addition to the dc circuit breaker, the ac side breakers of the respective MMC are tripped if a fault or overcurrent is detected.

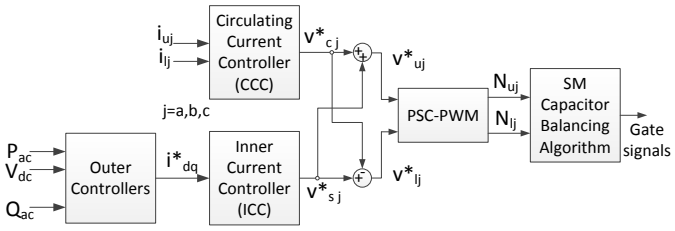

Fig. 9. Control structure of the MMC station, where u, l indicate the upper and lower arm of the MMC respectively and j indicates the corresponding phase leg [34].

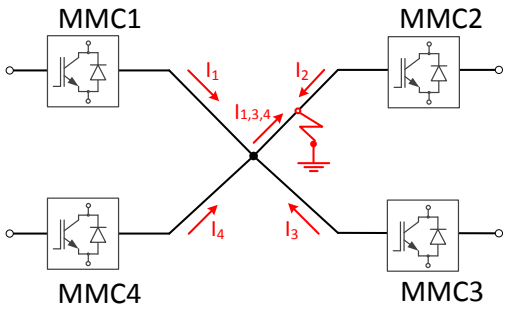

Fig. 10. Current direction during a dc fault [34].

TABLE IV
CIRCUIT BREAKER PARAMETERS.

Parameters	Unit	Value
Nominal Path Forward Resistance (R_n)	mΩ	1.5
Comm. Path Forward Resistance (R_c)	mΩ	288
UFD opening time (t_c)	ms	2
Number of IGBTs in CCP (n_c)	-	192
LCS Snubber Resistance (R_s)	Ω	100
LCS Snubber Capacitance (C_s)	uF	4
Breaker Snubber Resistance (R_b)	Ω	5000
Breaker Snubber Capacitance (C_b)	uF	4
Limiting inductance ($L_{1,2,3,4}$)	mH	30
Residual voltage of SA @ 10kA	pu	2.2

IV. RESULTS

In this Section, the operational dynamics of the two breaker concepts and the effect on the post-fault operation of the inter-

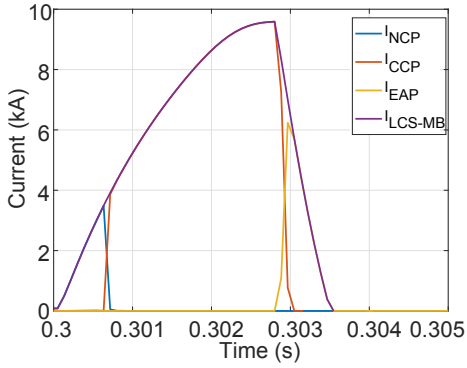

(a)

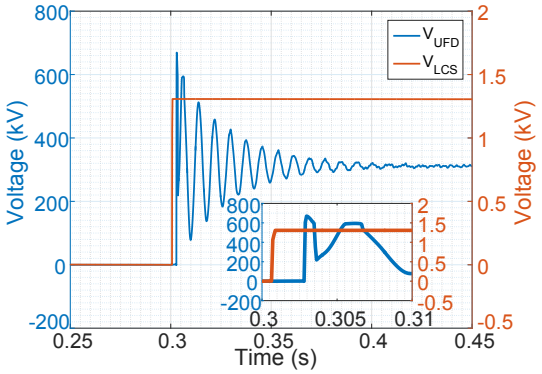

(b)

Fig. 11. LCS-MB: (a) current on the breaker paths; (b) voltage stresses on the NCP switches.

connected stations are evaluated. A dc fault with a resistance of 7 Ω is applied at 0.3 s of the simulation [11]. The worst-case scenario for the protection system coordination is when the fault occurs as close as possible to the central node of the grid and to the breaker station, as identified in [18]. A pole-to-ground dc fault is investigated to compare and evaluate the performance of the two breaker technologies. The fault is applied on line 2 as shown in Fig. 8 and Fig. 10. Breakers are placed on both poles of the dc grid and their operation is triggered by the same fault detection signal to completely isolate the faulty part of the grid.

The currents and voltages are monitored during simulation at all crucial points of the grid. The most important results showing the transients taking place during the dc fault are presented in Fig. 11 and Fig. 12 for the LCS-MB and the MLB, respectively.

The current that the LCS-MB needs to interrupt, reaches a peak of 9.6 kA in the CCP. As soon as the LCS is turned off, a commutation voltage builds up across the LCS leading to the current commutation into the CCP. The UFD is opened and after current interruption, it has to withstand the transient interruption voltage (TIV) with a peak of 671 kV and a steady-state value equal to the nominal dc pole voltage. Although the current drops to zero after almost 3.6 ms, the voltage takes approximately 60 ms to reach a steady-state. This can be attributed to the LC parameters of the dc lines and the transient response post-fault, as shown in Fig. 13.

In case of the MLB, the current and voltage stresses on the paths connected to the faulty line and the respective stresses on the paths connected to one 'healthy' line are presented in Fig. 12. The peak current on the main breaker path also reaches 9.6 kA, while the voltage on the surge arrester reaches a peak of 672 kV and a steady-state of 320 kV before dropping to zero when the faulty line is isolated and the main breaker is reset for later operation. The peak current is the same as in the case of LCS-MB, since the grid RLC parameters are the same. On the paths connected to the faulty line, the UFD takes up the voltage stress as in the case of the LCS-MB breaker, whereas the voltage across the LCS remains low. The respective path current drops to zero depending on the switching sequence of the MLB, as presented in Fig. 6.

In the healthy path 1a, the LCS and the UFD remain closed at all instants. As shown in Fig. 12 (a), initially there is a surge current resulting from the discharge of the capacitance of line 1 towards the dc fault point. The current dynamics follow the dc voltage dynamics in the grid. On path 1b, the voltage across the UFD reaches a peak of 670 kV as the path is disconnected for a time period until the fault is isolated. The current characteristics are similar to path 1a.

The overall system response is better evaluated by monitoring the dc voltage at the output of MMC1. From Fig. 13, it becomes apparent that the voltage transients taking place in both case studies are very similar, as they depend on the fault interruption time and the LC parameters of the 'healthy' cables, which get anew charged to their nominal voltage level after the fault is isolated. From the zoomed subfigure in Fig. 13, it can be seen that the voltage drop starts to recover at 3.1 ms and 3.2 ms for LCS-MB and MLB respectively, which

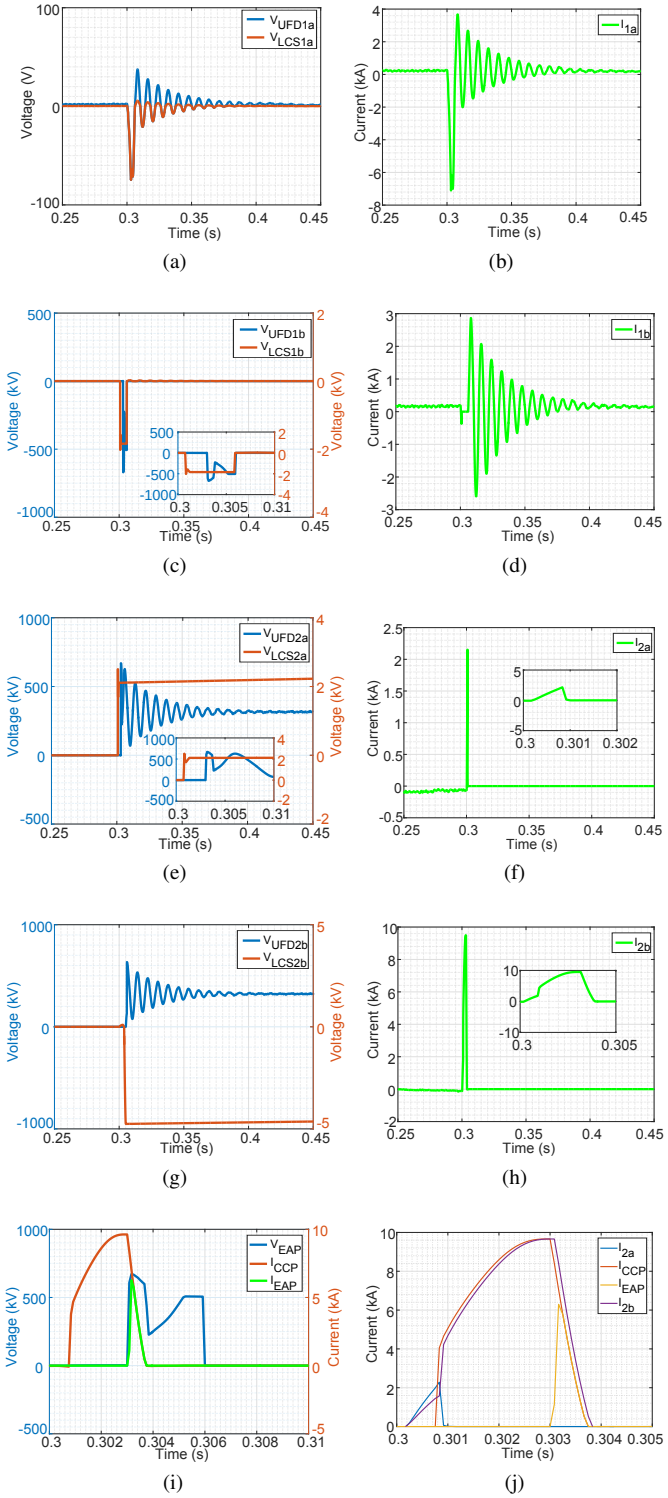

Fig. 12. Current and Voltage at the paths of MLB1: (a) Voltages on 'healthy' NCP 1a; (b) current on 'healthy' NCP 1a; (c) voltages on 'healthy' NCP 1b; (d) current on 'healthy' NCP 1b; (e) voltages on 'faulty' NCP 2a; (f) current on 'faulty' NCP 2a;(g) voltages on 'faulty' NCP 2b; (h) current on 'faulty' NCP 2b ;(i) CCP and EAP path; (j) Total breaker fault current.

is the time when the fault current is fully commutated to the surge arrester. In both cases the nominal voltage level reaches a new steady-state level post-fault after approximately 60 ms (t_{Vss}), while it is fully restored above 90% after 27 ms (t_{V90}).

For the case study under investigation, the switching se-

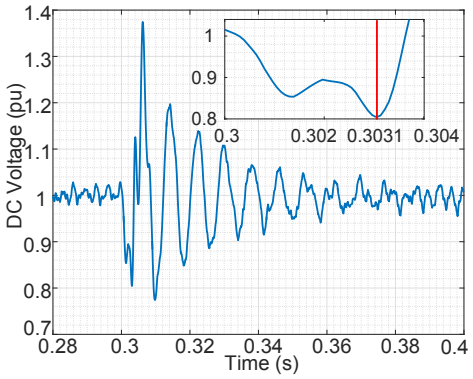

(a)

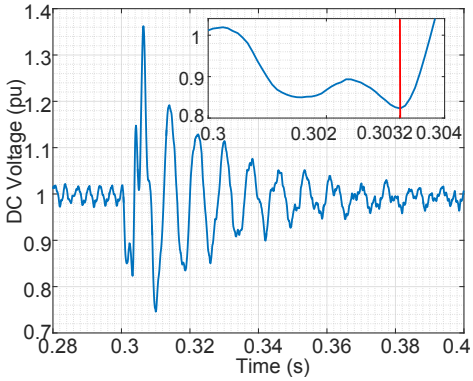

(b)

Fig. 13. DC voltage at MMC1: (a) LCS-MB; (b) MLB. The red line indicates the time at which the dc voltage starts to recover in each case.

quence in the breakers is presented in Table V, using the symbols introduced in Section II for the switching times. The fault detection time is the same for both systems, since it only depends on the grid and fault characteristics. Moreover, the total interruption time $t_{\text{Interruption}}$ for MLB is higher by 0.2 ms compared to LCS-MB. This difference can be attributed to the fact that in MLB the current in multiple NCP paths needs to drop to a residual current level before the CCP can be switched off.

Table VI compares the most important aspects of the breaker operation. In fact, the LCS-MB and the MLB experience similar peak currents in the CCP (∼9.6 kA). However, it has to be noted that a change in the current rating of the CCP can have a significant impact on the design of the breaker and its cost. Considering a case study in which the peak current would increase over 12 kA, assuming that the IGBTs have a current rating of 3 kA [36], a whole new stack of IGBTs needs to be added in parallel to the CCP path to withstand the peak current. As a result, 96 new IGBTs need to be added in the CCP path of the MLB, while this number is quadrupled in case of the LCS-MB, since the CCP path of the LCS-MB on each line needs to be rated for the new current peak.

On the other hand, 213.1% higher current peak is reached in NCP path 2b of MLB, as this needs to remain connected to the faulty line until the breaker operation has brought current to zero. Although there is a considerable difference in the relative change, the consequences are fundamentally different compared to the CCP case due to the low voltage rating of the LCS. Because of the low current on the NCP path of LCS-MB, two parallel stacks of three series-connected IGBTs are sufficient. On the contrary, the MLB needs four parallel stacks of three series-connected IGBTs on each NCP. In fact, the number of additional IGBTs on the NCP of MLB has to be scaled by the number of parallel connected IGBTs and by twice the number of connected lines. As a result, the MLB needs in total 48 IGBTs (six on each of the eight NCPs) more than the LCS-MB. Hence, while still considerable, it is a minor increase compared to the number of additional CCPs (192 IGBTs each) of the LCS-MB configuration. It has to be noted that the design aspects are case specific (semiconductor selection, grid configuration, fault type etc.) and are hereby provided as examples of system designer considerations.

Finally, the energy absorption on the EAP path in the LCS-MB is similar to the MLB, since the fault current is similar. As a result, the surge arresters are dimensioned the same. The advantage of MLB is that in case resizing is necessary, the cost and complexity of the task is lower, since only one EAP is used for each dc node. However, reduced lifetime of the surge arrester might be expected, as it is activated more often in MLB than in case of multiple LCS-MBs.

V. Conclusions

This paper analyzed a breaker arrangement, named the Multi-Line Breaker (MLB), for the successful fault isolation in MTdc networks. The breaker can be used in dc nodes connecting multiple lines and was proven to isolate faults bidirectionally in any of the interconnected lines using a single main breaker path in a unidirectional configuration. Due to the limited hardware requirements, it is easy to implement the MLB using hybrid breakers as the basis for its design, while at the same time it constitutes a more cost-effective solution,

TABLE V
Switching Sequence Events.

Time	LCS-MB	MLB
t_{Det} (ms)	0.6	0.6
t_{LCS} (ms)	0.6	-
t_{UFD} (ms)	0.8	-
t_{CCP} (ms)	2.8	3
$t_{\text{Interruption}}$ (ms)	**3.6**	**3.8**
t_{Vss} (ms)	**60**	**60**
t_{V90} (ms)	**27**	**27**
$t_{\text{LCS-nf(a)}}$ (ms)	-	0.7
$t_{\text{LCS-f(a)}}$ (ms)	-	0.7
$t_{\text{LCS-f(b)}}$ (ms)	-	3.7
$t_{\text{UFD-nf(a)}}$ (ms)	-	0.9
$t_{\text{UFD-f(a)}}$ (ms)	-	0.9
$t_{\text{UFD-f(b)}}$ (ms)	-	3.7
$t_{\text{r(LCS-nf(b))}}$ (ms)	-	5.7
$t_{\text{r(UFD-nf(b))}}$ (ms)	-	5.8
$t_{\text{r-CCP}}$ (ms)	-	5.8

TABLE VI
BREAKER COMPARISON.

Peak Values	LCS-MB	MLB	MLB-p Path	% Diff.
V_{LCS} (kV)	1.52	4.76	2b	213.1
V_{UFD} (kV)	670	670	1b	0
V_{EAP} (kV)	671	672	-	0.1
I_{NCP} (kA)	3.46	9.62	2b	178
I_{CCP} (kA)	9.6	9.62	-	0.2
I_{EAP} (kA)	6.19	6.26	-	1.13
$E_{\text{absorption}}$ (MJ)	1.33	1.39	-	4.5

especially in cases where a high number of lines is connected to the same grid node. The comparison between the MLB concept and the use of hybrid breakers for each dc line showed that the overall system dc fault response is similar and thus, the MLB is a promising alternative for the dc fault isolation.

While the MLB concept is not suggested for point-to-point connections, it can be applied in all types of grid configurations, as long as there is a node in the network connecting multiple lines. The design of the breaker is highly modular with minimum control additions and can, therefore, easily accommodate the addition of future dc lines to an existing grid.

REFERENCES

[1] K. Meah and S. Ula, "Comparative Evaluation of HVDC and HVAC Transmission Systems," in *Power Engineering Society General Meeting, 2007. IEEE*, June 2007, pp. 1–5.

[2] M. Sleiman, A. Al Hage Ali, H. F. Blanchette, K. Al-Haddad, B. Piepenbreier, and H. Kanaan, "A survey on modeling, control, and dc-fault protection of modular multilevel converters for HVDC systems," in *Industrial Electronics (ISIE), 2014 IEEE 23rd International Symposium on*, June 2014, pp. 2149–2154.

[3] Y. Xue and Z. Xu, "On the Bipolar MMC-HVDC Topology Suitable for Bulk Power Overhead Line Transmission: Configuration, Control, and DC Fault Analysis," *Power Delivery, IEEE Transactions on*, vol. 29, no. 6, pp. 2420–2429, Dec 2014.

[4] R. T. Pinto, S. F. Rodrigues, E. Wiggelinkhuizen, R. Scherrer, P. Bauer, and J. Pierik, "Operation and power flow control of multi-terminal dc networks for grid integration of offshore wind farms using genetic algorithms," *Energies*, vol. 6, no. 1, pp. 1–26, 2012. [Online]. Available: http://www.mdpi.com/1996-1073/6/1/1

[5] D. Jovcic, D. Van Hertem, K. Linden, J. P. Taisne, and W. Grieshaber, "Feasibility of DC transmission networks," in *Innovative Smart Grid Technologies (ISGT Europe), 2011 2nd IEEE PES International Conference and Exhibition on*, Dec 2011, pp. 1–8.

[6] M. K. Bucher, R. Wiget, G. Andersson, and C. M. Franck, "Multiterminal HVDC Networks: What is the Preferred Topology?" *Power Delivery, IEEE Transactions on*, vol. 29, no. 1, pp. 406–413, Feb 2014.

[7] S. Rodrigues, R. T. Pinto, P. Bauer, and J. Pierik, "Optimal Power Flow Control of VSC-Based Multiterminal DC Network for Offshore Wind Integration in the North Sea," *Emerging and Selected Topics in Power Electronics, IEEE Journal of*, vol. 1, no. 4, pp. 260–268, Dec 2013.

[8] G. Tang, Z. He, H. Pang, X. Huang, and X. P. Zhang, "Basic topology and key devices of the five-terminal dc grid," *CSEE Journal of Power and Energy Systems*, vol. 1, no. 2, pp. 22–35, June 2015.

[9] B. Geebelen, W. Leterme, and D. Van Hertem, "Analysis of DC breaker requirements for different HVDC grid protection schemes," in *AC and DC Power Transmission, 11th IET International Conference on*, Feb 2015, pp. 1–7.

[10] E. Kontos, R. T. Pinto, S. Rodrigues, and P. Bauer, "Impact of hvdc transmission system topology on multiterminal dc network faults," *Power Delivery, IEEE Transactions on*, vol. 30, no. 2, pp. 844–852, April 2015.

[11] M. K. Bucher and C. M. Franck, "Contribution of Fault Current Sources in Multiterminal HVDC Cable Networks," *Power Delivery, IEEE Transactions on*, vol. 28, no. 3, pp. 1796–1803, July 2013.

[12] M. Hajian, D. Jovcic, and B. Wu, "Evaluation of Semiconductor Based Methods for Fault Isolation on High Voltage DC Grids," *Smart Grid, IEEE Transactions on*, vol. 4, no. 2, pp. 1171–1179, June 2013.

[13] E. Kontos, R. T. Pinto, and P. Bauer, "Effect of power flow control methods on the dc fault response of multi-terminal dc networks," in *Industrial Electronics Society, IECON 2014 - 40th Annual Conference of the IEEE*, Oct 2014, pp. 2075–2081.

[14] Y. Wang and R. Marquardt, "Future hvdc-grids employing modular multilevel converters and hybrid dc-breakers," in *Power Electronics and Applications (EPE), 2013 15th European Conference on*, Sept 2013, pp. 1–8.

[15] K. Sano and M. Takasaki, "A Surgeless Solid-State DC Circuit Breaker for Voltage-Source-Converter-Based HVDC Systems," *Industry Applications, IEEE Transactions on*, vol. 50, no. 4, pp. 2690–2699, July 2014.

[16] U. Amir Khan, J.-G. Lee, F. Amir, and B.-W. Lee, "A Novel Model of HVDC Hybrid-Type Superconducting Circuit Breaker and Its Performance Analysis for Limiting and Breaking DC Fault Currents," *Applied Superconductivity, IEEE Transactions on*, vol. 25, no. 6, pp. 1–9, Dec 2015.

[17] K. Tahata, S. E. Oukaili, K. Kamei, D. Yoshida, Y. Kono, R. Yamamoto, and H. Ito, "HVDC circuit breakers for HVDC grid applications," in *AC and DC Power Transmission, 11th IET International Conference on*, Feb 2015, pp. 1–9.

[18] E. Kontos, S. Rodrigues, R. T. Pinto, and P. Bauer, "Optimization of limiting reactors design for dc fault protection of multi-terminal hvdc networks," in *Energy Conversion Congress and Exposition (ECCE), 2014 IEEE*, Sept 2014, pp. 5347–5354.

[19] C. M. Franck, "HVDC Circuit Breakers: A Review Identifying Future Research Needs," *Power Delivery, IEEE Transactions on*, vol. 26, no. 2, pp. 998–1007, April 2011.

[20] J. Häfner and B. Jacobson, "Proactive Hybrid HVDC Breakers - A key innovation for reliable HVDC grids," in *The Electric Power System of the Future - Integrating supergrids and microgrids, Cigré International Symposium*, Bologna, Italy, 13-15 September 2011.

[21] W. Grieshaber, J.-P. Dupraz, D. L. Penache, and L. Violleau, "Development and test of a 120 kV direct current circuit breaker," in *Cigré Session*, Paris, France, 2014.

[22] Y. Wang and R. Marquardt, "A fast switching, scalable DC-Breaker for meshed HVDC- SuperGrids," in *PCIM Europe*, Nürnberg, Germany, 2014.

[23] T. Schultz, V. Lenz, and C. M. Franck, "Circuit Breakers for Fault Current Interruption in HVDC Grids," in *VDE-Fachtagung Hochspannungstechnik*, Berlin, Germany, 2016.

[24] J. Fu, Z. Yuan, Y. Wang, S. Xu, W. Wei, and Y. Luo, "Control strategy of system coordination in Nanao multi-terminal VSC-HVDC project for wind integration," in *PES General Meeting — Conference Exposition, 2014 IEEE*, July 2014, pp. 1–5.

[25] G. Tang, Z. He, H. Pang, X. Huang, and X.-P. Zhang, "Basic topology and key devices of the five-terminal DC grid," *Power and Energy Systems, CSEE Journal of*, vol. 1, no. 2, pp. 22–35, June 2015.

[26] D. Jovcic, M. Taherbaneh, J. Taisne, and S. Nguefeu, "Topology assessment for 3 + 3 terminal offshore dc grid considering dc fault management," *Generation, Transmission Distribution, IET*, vol. 9, no. 3, pp. 221–230, 2015.

[27] A. N. Greenwood and T. H. Lee, "Theory and application of the commutation principle for hvdc circuit breakers," *IEEE Transactions on Power Apparatus and Systems*, vol. PAS-91, no. 4, pp. 1570–1574, July 1972.

[28] R. Majumder, S. Auddy, B. Berggren, G. Velotto, P. Barupati, and T. U. Jonsson, "An alternative method to build dc switchyard with hybrid dc breaker for dc grid," *IEEE Transactions on Power Delivery*, vol. 32, no. 2, pp. 713–722, April 2017.

[29] L. Mackay and E. Kontos, "DC switch yard and method to operate such a DC switch yard," Patent: WO 2017/034408 A1, 2017.

[30] F. Xu, H. Yu, Y. Lu, P. Qiu, K. Tong, J. Xuan, Q. Chen, X. Huang, and D. Jiang, "Topology, control and fault analysis of a new type HVDC breaker for HVDC systems," in *2016 IEEE PES Asia-Pacific Power and Energy Engineering Conference (APPEEC)*, Oct 2016, pp. 1959–1964.

[31] M. Callavik, A. Blomberg, J. Häfner, and B. Jacobson, "The Hybrid HVDC Breaker: An innovation breakthrough enabling reliable HVDC grids," ABB Grid Systems, Tech. Rep., 2012.

[32] K. Sharifabadi, L. Harnefors, H.-P. Nee, S. Norrga, and R. Teodorescu, *Design, Control and Application of Modular Multilevel Converters for HVDC Transmission Systems*, 1st ed. John Wiley & Sons, Ltd., 2016.

[33] K. Ilves, S. Norrga, L. Harnefors, and H. P. Nee, "On Energy Storage Requirements in Modular Multilevel Converters," *IEEE Transactions on Power Electronics*, vol. 29, no. 1, pp. 77–88, Jan 2014.

[34] E. Kontos, R. T. Pinto, and P. Bauer, "Providing dc fault ride-through capability to H-bridge MMC-based HVDC Networks," in *Power Electronics and ECCE Asia (ICPE ECCE), 2015 IEEE 9th International Conference on*, June 2015.

[35] A. Hassanpoor, J. Häfner, and B. Jacobson, "Technical Assessment of Load Commutation Switch in Hybrid HVDC Breaker," *IEEE Transactions on Power Electronics*, vol. 30, no. 10, pp. 5393–5400, Oct 2015.

[36] ABB Switzerland Ltd., "5SNA 3000K452300 StakPak IGBT Module datasheet," Online, Dec 2015.